



Removal of Congo red from aqueous solutions by adsorption onto illite clay

Omar T.S. Altaie^a, Hani Zeidan^{a,b}, Necati Karakaya^c, Muazzez Ç. Karakaya^c,
Mustafa E. Marti^{a,b,*}

^aDepartment of Chemical Engineering, Selcuk University, Konya, Turkey

^bDepartment of Chemical Engineering, Konya Technical University, Konya, Turkey, Tel.: +90-332-223-2304; Fax: +90-332-241-0635; email: memarti@ktun.edu.tr

^cDepartment of Geological Engineering, Konya Technical University, Konya, Turkey

Received 16 March 2023; Accepted 2 September 2023

ABSTRACT

Many synthetic dyes are toxic and must be removed from industrial effluents to prevent critical environmental and health problems. Adsorptive technologies are favored and several adsorbents have been tested for this purpose. Efficiency, economic suitability, and environmental compatibility are the most critical criteria in the selection of an adsorbent. The focus of the present study was the adsorption of Congo red (CR), an anionic diazo dye, from aqueous solutions using illite mineral. The Brunauer–Emmett–Teller surface area of the mineral tested in the study was 44.73 m²/g. Solution pH had a significant effect on the process, with the highest adsorption efficiency (AE) at pH 5.7. The process reached equilibrium after 2 h and the relevant data were in good agreement with the pseudo-second-order kinetic model. Adsorption efficiency decreased with temperature; the process was exothermic and non-spontaneous, according to thermodynamic data. The isotherm curves were fitted with Type I adsorption, and adsorption capacity increased with illite dosage but was negatively impacted by initial CR concentration. The highest adsorption capacity was 61.02 mg/g, and the equilibrium data were well described ($R^2 = 0.999$) by the Langmuir isotherm model. This study demonstrates that illite mineral can be used for the remediation of the anionic diazo dye Congo red by adsorption.

Keywords: Illite; Clay mineral; Congo red; Adsorption

1. Introduction

Dyes are widely used in many industries to improve the aesthetic impact of products and to protect them from external factors [1]. Most industrial dyes contain aromatic moieties (i.e., azo functional groups) that have human toxicity. In addition, dyeing processes usually generate significant volumes of colored wastewater that require proper remediation [2]. Discharge of these painted effluents into rivers and other bodies of water can be a threat to the environment and human health [3].

Azo dyes are used extensively in industry. Most of these colorants are reported to be toxic, carcinogenic, mutagenic, and environmentally unfriendly. Their toxicity, which can persist for years [4] is mainly due to the aromatic moieties in their structures and may be caused by the dye itself or its metabolites. For this reason, the use of azo dyes has been restricted in many countries.

Congo red (CR) is a commonly used industrial azo dye. It was discovered by Paul Bottinger in 1884 and has two azo ($-N=N-$) chromophores and acidic auxochromes ($-SO_3H$) bonded to benzene moieties [5]. Following cleavage of the azo groups, the dye colorant may degrade into benzidine,

* Corresponding author.

a highly carcinogenic amine. Congo red is also mutagenic, teratogenic, or toxic to a variety of organisms, including humans, plants, animals, bacteria, algae, protozoa, and parasites. The degree of toxicity varies depending on the concentration, type of metabolite and organism [6,7]. Because of this, CR's application as a dye is restricted, although it is broadly used in textiles, wood, pigments, pharmaceuticals, leather, cosmetics, food, and paper.

Like other industrial wastes, dyes must be removed from effluents before they are discharged. Coagulation, flocculation, membrane filtration, reverse osmosis, filtration, and adsorption have been tested for this purpose [8–10]; the latter is favored due to its high affinity, relatively lower cost, eco-friendly nature, reusability, and inert process elements [11–13]. The process can be operated continuously via appropriate column systems [14–16]. Inert and non-toxic materials are usually preferred with activated carbon (AC) considered the most efficient adsorbent for the purpose [16–21]. However, new alternatives require evaluation due to the relatively high production and regeneration costs of AC [22,23].

Due to their unique layered atomic structure, high aspect ratio, and abundance of chemically active surface sites, clay and zeolite minerals have a great potential to adsorb materials from liquid or gaseous media [24,25]. Some clay minerals, for example, montmorillonite, kaolinite and sepiolite, and zeolite minerals, for example, chabazite and clinoptilolite are naturally-occurring materials that have been tested for remediation of heavy metals, toxic dyes and complex organics in aqueous-based solutions [8,26–29]. Illite is a clay mineral that usually forms in sedimentary rocks by hydrothermal alteration or diagenetic processes through illitization of other clay, mica, or feldspar minerals [30–34]. The formation of illite occurs in three ways: (1) classical recrystallization of smectite to illite, (2) direct precipitation from solution on kaolinite or quartz surfaces, and (3) degradation or alteration of mica or feldspar minerals [32]. Illite is comprised of two tetrahedral silica layers and one octahedral layer (2:1) with the general formula of $K_Y Al_4 [Si_{8-Y} Al_Y O_{20}] (OH)_4$. The value of Y in the formula lies between 1 and 1.5 [33,34]. Due to the inequality of the charges, Si^{+4} (silicon) ions are replaced by Al^{+3} (aluminum) ions. This results in formation of high negative charges in the tetrahedral sheets [35] that are mainly balanced by K^+ ions, and to a lesser extent, Na^+ , Cs^+ , and NH_4^+ ions; the first K^+ can be substituted by Mg^{2+} and Ca^{2+} ions. The presence of potassium ions between the layers prevents penetration by water, thus limiting the expansion of illite [36].

In this study, illite, a phyllosilicate or a layered aluminosilicate, was tested as an adsorbent for the removal of CR from aqueous solutions. Kinetic, isotherm, and thermodynamic analyses were performed. The effects of process parameters were examined and the adsorption mechanism was explained using various models.

2. Materials and methods

2.1. Materials

The illite used in the experiments was obtained from the northwest of Ordu in Turkey. The mineralogical,

chemical, and physical properties of the illite were previously determined [37]. This mineral is of high purity, bright white (whiteness degree: 45–78) and was used without pre-treatment except sieving (particle size <53 mesh). Aqueous solutions were prepared using ultra-high pure (UHP) water obtained from a Merck Millipore Direct-Q 3V System (USA). Congo red (CR), a benzidine-based anionic diazo dye, has the empirical formula $C_{23}H_{22}N_6O_6S_2Na_2$. Its properties and structure are shown in Table S1 and Fig. 1, respectively. The pH of aqueous solutions was adjusted as needed with NaOH and HCl. All chemicals used in the experiments were analytical grade and supplied by Merck Co., USA.

2.2. Characterization

Total contents of the major oxides were determined using ICP-MS. Loss of ignition (LOI) was performed at ACME Laboratories (Canada) by measuring the difference in weight after ignition at 1,000°C. The functional groups on the illite surface were identified using a Bruker-Platinum ATR-Vertex 70FTIR (Bruker, Germany). The Brunauer–Emmett–Teller (BET) surface area of the sample was determined using a TriStar II-3020 (Micromeritics, USA); analyses were done within the range of 4,000–400 cm^{-1} . The surface properties and elemental percentage of the illite sample were investigated by a scanning electron microscopy (SEM) + energy-dispersive X-ray (EDX) spectroscopy (SEM, Zeiss, Germany; EDX, Bruker, Germany) combined system.

2.3. Experimental methods

2.3.1. Preparation of aqueous phases and experimental procedure

A concentrated stock solution of CR was prepared by dissolving 1 g of dye powder in 1 L UHP water, then used to prepare the aqueous phases. In the experiments, initial CR concentrations ranged from 25 to 500 mg/L.

Adsorption experiments were carried out by contacting 10 mL aqueous CR solutions with illite at predetermined dosage levels (1–5 g/L) in Erlenmeyer flasks. The phases were shaken at 150 rpm for 2 h until equilibrium was obtained. Mixtures were then centrifuged at 6,000 rpm for 2 min to obtain clear solid–liquid phase separations. The aqueous phase was carefully removed for quantitation of CR concentration.

2.3.2. Quantitative analysis and calculation

The CR concentration in the liquid phase was analyzed by a UV-spectrometer (Shimadzu UVmini-1240). The maximum absorbance for CR was 497 nm. Initial (C_0) and

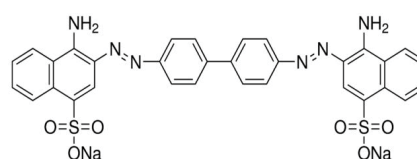


Fig. 1. Structure of Congo red.

equilibrium (C_e) concentrations of CR were used during the calculation of adsorption capacity and efficiency.

2.3.3. Effect of solution pH

The pH effect was investigated in the pH range of 5.7–10.5 using CR solutions with an initial concentration of 100 mg/L; the original pH of the aqueous CR solution was 7.5. The pH range was chosen based on previous studies and analysis limitations. The pH adjustments were made using HCl and NaOH. The pH at the zero-charge point (pH_{pzc}), where the adsorbent surface is neutral, was determined according to Balistrieri and Murray [38]. 40 mL of 0.01 M NaNO_3 were added to 100 mL Erlenmeyer flasks. Initial pH values (pH_i) were adjusted over the range of 2–11 with HCl or NaOH. The final volumes were adjusted to 50 mL with 0.01 M NaNO_3 , followed by the addition of 0.01 g of illite. The flasks were sealed and the suspensions shaken in a water bath at 298 K and 150 rpm for 48 h, after which the final pH (pH_f) values of the supernatant liquids were measured. The differences (ΔpH) between pH_f and pH_i values were plotted vs. initial pH and the intersection of the resulting curve with the x-axis defines the pH_{pzc} of illite [38].

2.3.4. Kinetic studies

Illite suspensions in aqueous CR were prepared in 50 mL Erlenmeyer flasks. Each flask contained 10 mL of CR solution at a concentration of 100 mg/L; the dosage of illite was fixed at 1 g/L. The 20 flasks were shaken at 150 rpm and 298 K over a period of 5 h. At pre-determined intervals, the flask contents were harvested by centrifugation and the clarified supernatants analyzed for residual CR concentrations as previously described. Kinetic data were evaluated using four kinetic models: (1) Elovich, (2) pseudo-first-order, (3) pseudo-second-order, (4) Weber–Morris intraparticle diffusion.

2.3.5. Thermodynamic studies

To observe the effect of temperature on the adsorption process and calculate thermodynamic parameters, experiments were performed at different temperatures (298, 318,

and 338 K). The adsorbent dose was maintained at 1 g/L; initial CR concentrations ranged from 25 to 500 mg/L. Changes in Gibbs free energy, enthalpy, and entropy were calculated using the relevant data.

2.3.6. Isotherm studies

The effects of CR concentration and illite dose on the adsorption efficiency (AE) and capacity were examined. Four different isotherm models were used to interpret the relevant data. The adsorbent dosages and CR concentrations ranged from 1–5 g/L and 25–500 mg/L, respectively. Experiments were conducted at 298 K for 2 h. At equilibrium, the samples were clarified by centrifugation and the resulting supernatants were analyzed for CR concentration. Langmuir, Freundlich, Temkin, and Dubinin–Radushkevich isotherm models were applied to the data to elucidate the interactions between CR and illite.

3. Results and discussion

3.1. Characterization

The functional groups on the illite surface were identified by Fourier-transform infrared spectroscopy (FTIR) analysis using the samples before and after the experiments [39,40]. The FTIR spectra show peaks at 475.92, 533.77, 758, 822, 918, 1,021.98 and 3,620 cm^{-1} (Fig. 2). The latter peak is attributed to the OH stretching band. Absorption bands between 400 and 1,200 cm^{-1} are typically due to vibrations of the aluminosilicate structure; strong Si–O bands are observed at 1,000 cm^{-1} [41]. The bands at 533 and 758 cm^{-1} refer to the stretching of Al–O–Si group, while those at 475.92 cm^{-1} represents bending vibrations of Si–O–Si group. The signal at 1,021.98 cm^{-1} is attributed to the stretching of the Si–O group. The bands at 918 and 822 cm^{-1} are associated with the stretching vibrations of Al–OH and Al–O groups [42].

The peak intensities slightly decreased after CR adsorption (Fig. 2). The decrease is maximal for the peak at 1,021.98 cm^{-1} (Si–O), indicating a relatively more important role of this functional group in the process. The peak of the OH group at 3,620 cm^{-1} disappeared after the process.

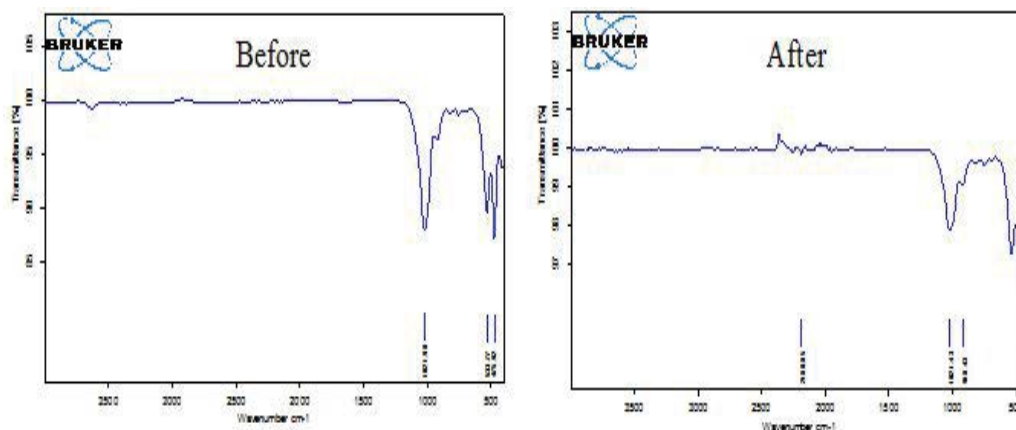


Fig. 2. FTIR spectra of illite before and after adsorption of Congo red.

All the changes in the strength of the peaks can be linked to the adsorption process [43].

The BET surface area of the illite was found to be 44.73 m²/g. The morphology of illite was investigated by SEM (Fig. S1). It was observed that illite may be transformed from a smectitic clay with a leaf-like or broad honeycomb habit [44]. The chemical composition of the illite used in this study is given in Table S2. EDX data show that it is composed mainly of oxygen, silicon, aluminum, and potassium (Table S3); minor amounts of carbon, magnesium, iron, titanium, sulfur, and sodium are also present.

3.2. Effect of initial pH

The pH of the aqueous medium is one of the most important parameters of adsorption processes as it affects both the adsorbent surface's charge and the dissociation of the solutes in the aqueous phase [23]. Therefore, AE can be influenced by solution pH. The effect of pH can be estimated by the material's point zero charge (pH_{pzc}) [40,45], or the pH at which negative and positive charges are equal on the adsorbent's surface. The latter is positively charged at pH < pH_{pzc} but negatively charged at pH > pH_{pzc}. Fig. 3 shows that pH_{pzc} for illite is ~pH 7, which is consistent with previous reports [46].

The effect of pH on CR adsorption onto illite was investigated using aqueous solutions with initial CR concentrations of 100 mg/L at pH 7.5. The illite dosage was maintained at 1 g/L; the effect of pH was examined in the range of 5.7–10.5. Fig. 3 shows that the AE decreased from 51.1% to 26.7% over this range. The initial pH had a significant effect on CR adsorption (Table S4), most likely due to the dissociation of the siloxane (Si–O–Si) and other functional groups at higher pH. This resulted in a more negatively charged illite surface (pH > pH_{pzc}). Repulsive forces between the CR and illite surface are most likely responsible for the lower yields [40,47,48].

3.3. Determination of equilibration time

Contact time is another critical parameter that affects AE. Information on kinetics is required for the design of a process and equilibration time must be determined. Kinetic

trials were conducted over 300 min using aqueous solutions with initial CR concentrations of 100 mg/L and illite at a dosage of 1 g/L. Fig. 4 shows that ≥75% of the CR was adsorbed onto illite during the first 10 min. The main reason for the high loading and rapid adsorption during this time was due to the abundance of unoccupied free silanol (Si–OH), siloxane (Si–O–Si), and other functional groups on the adsorbent surface. As these groups became saturated, adsorption slowed; the trend continued until equilibrium was reached at ~120 min (Fig. 4).

3.4. Kinetic models

The kinetic approach employs model expressions and relevant plots to estimate rate constants and describe the mechanism of the adsorption process [49,50]. The extent of the relationship between the process or kinetic data and the kinetic model was estimated using the determination coefficient (*R*²). Elovich, pseudo-first-order, pseudo-second-order, and intraparticle diffusion models [Eqs. (1)–(4)] are the most widely used kinetic models in literature [51–54].

$$\text{Pseudo-first-order: } \log(q_e - q_t) = \log q_e - \left(\frac{k_1}{2.303}\right) \cdot t \quad (1)$$

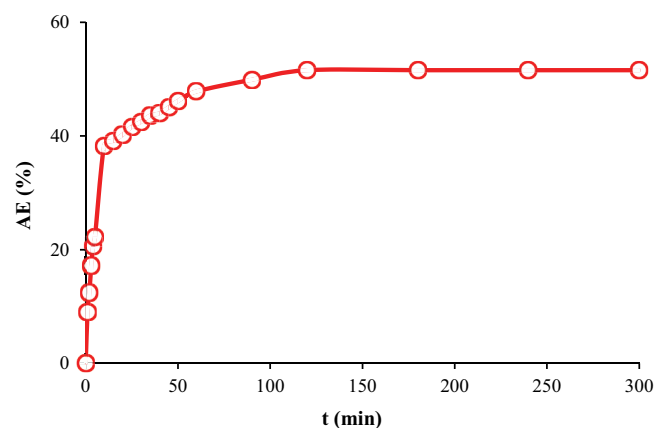


Fig. 4. Effect of contact time on the adsorption of Congo red by illite ([CR] = 100 mg/L, dose = 1 g/L, pH = 5.7, *T* = 298 K).

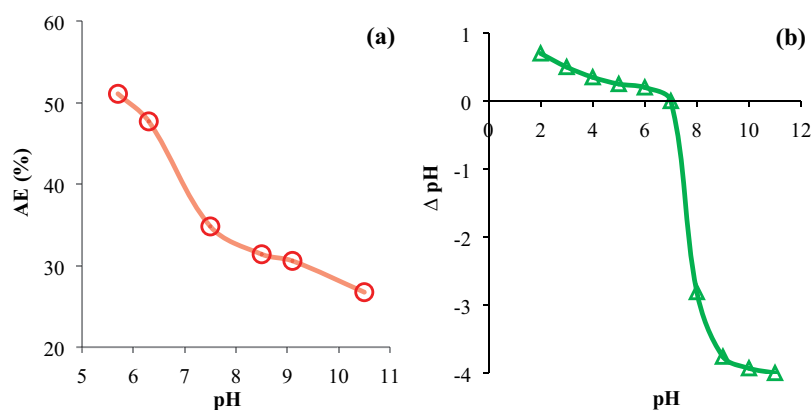


Fig. 3. (a) Effect of aqueous solution pH on the adsorption efficiency of Congo red onto illite clay. (b) Determination of the point zero charge (pH_{pzc}) of illite clay. ([CR] = 100 mg/L, dose = 1 g/L, *T* = 298 K).

$$\text{Pseudo-second-order: } \frac{t}{q_t} = \left(\frac{1}{k_2 \cdot q_e^2} \right) + \left(\frac{1}{q_e} \right) \cdot t \quad (2)$$

$$\text{Elovich: } q_t = \beta \cdot \ln(\alpha \cdot \beta) + \beta \cdot \ln(t) \quad (3)$$

$$\text{Intraparticle diffusion: } q_t = K_{id} \cdot t^{0.5} + I \quad (4)$$

Fig. 5 and Table 1 show that the highest R^2 (0.9984) was obtained with pseudo-second-order kinetics, indicating that the data are in good agreement with this model. The adsorption capacity was calculated as 53.19 mg/g and

was nearly identical to that determined experimentally ($q_e = 52.08 \text{ mg/g}$). The R^2 values from the pseudo-first-order and Elovich kinetic models were relatively low. According to the intraparticle diffusion model, CR adsorption consists of multiple stages. Since external film resistance (I) did not equal zero, intraparticle diffusion was not the only controlling mechanism [40,55].

3.5. Temperature effect and thermodynamic studies

The effect of temperature on CR adsorption was examined at 298, 318, and 338 K; the initial CR concentration ranged from 25 to 500 mg/L while illite dosage was

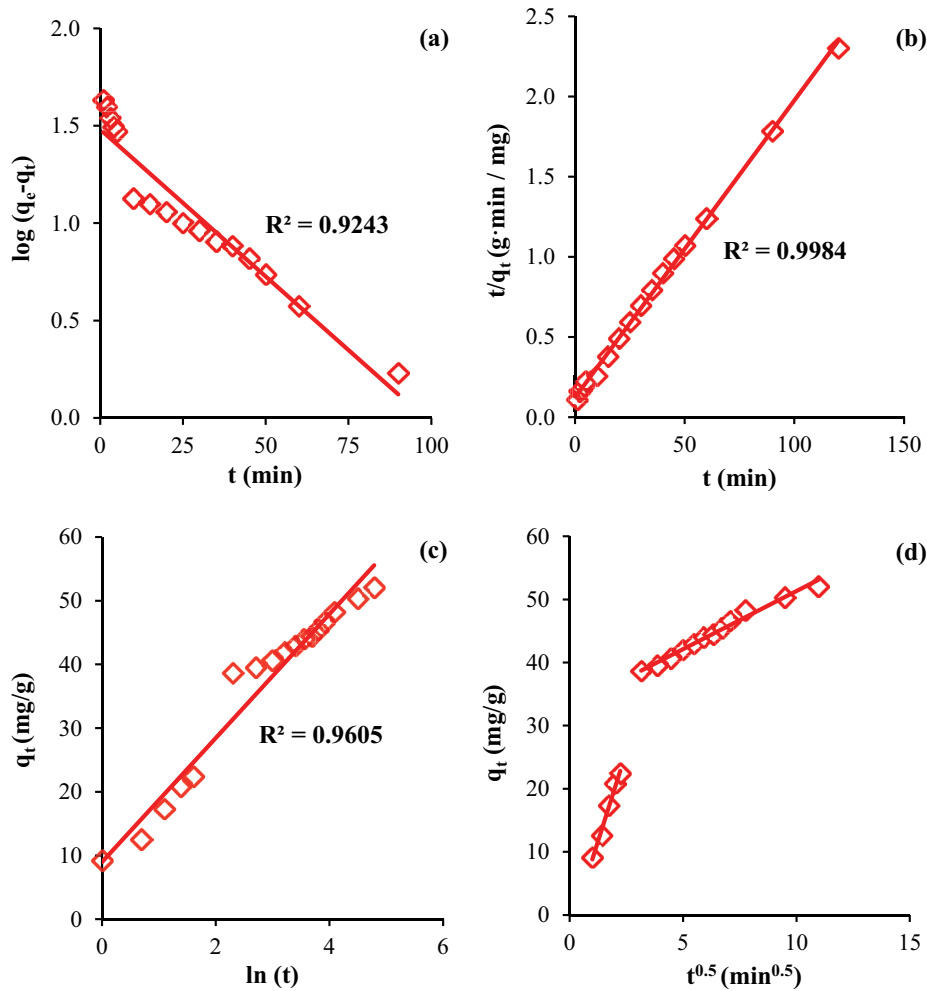


Fig. 5. Plots of kinetic models for the adsorption of Congo red by illite (a) pseudo-first-order, (b) pseudo-second-order, (c) Elovich, (d) intraparticle diffusion.

Table 1
Kinetic parameters for the adsorption of Congo red by illite

$q_{e(\text{exp})}$ (mg/g)	Pseudo-first-order			Pseudo-second-order			Elovich			Intraparticle diffusion	
	k_1 (1/min)	$q_{e(\text{cal})}$ (mg/g)	R^2	k_2 (g/mg·min)	$q_{e(\text{cal})}$ (mg/g)	R^2	α	β	R^2	K_{id} (mg/g·min ^{0.5})	I (mg/g)
52.08	0.03477	4.40	0.924	0.002787	53.19	0.998	0.259	9.725	0.960	2.8438	20.99

maintained at 1 g/L. In these trials, the initial aqueous pH was adjusted to 5.7. Fig. S2 shows that increasing temperature had an insignificant effect on CR deposition on illite (Table S4). This is likely due to the exothermic nature of the separation process. Higher temperatures may have decreased the van der Waals interactions between CR and illite [56,57].

The changes in Gibbs free energy (ΔG°) of the adsorption process were calculated using Eq. (5) and the data in Fig. S2. The overall changes in enthalpy (ΔH°) and entropy (ΔS°) were also determined by the graph of $\ln K_L$ vs. $1/T$ and Eq. (6). The results are summarized in Table 2.

$$\Delta G^\circ = -R \cdot T \cdot \ln K_L \quad (5)$$

$$\ln K_L = -\left(\frac{\Delta H^\circ}{R \cdot T}\right) + \frac{\Delta S^\circ}{R} \quad (6)$$

The type of interaction can be estimated according to the ΔG° values. For a physical adsorption process, ΔG° is between -20 and 0 kJ/mol, however ranges from -80 to -400 kJ/mol for chemical adsorption processes. Ruthven [59] stated that ΔH° values for physical and chemical adsorption processes vary in the ranges of 5 – 25 kJ/mol and 50 – 500 kJ/mol, respectively [58,59]. According to Table 2, ΔG° varied between 8.16 and 5.94 kJ/mol·K, indicative of physical interactions between CR and the illite surface. The negative and positive values of ΔH° and ΔG° signified the exothermic and non-spontaneous nature of the adsorptive separation process, respectively [60,61]. Moreover, negative ΔS° denotes the decreased randomness at the interface during CR adsorption [12,40].

3.6. Effects of initial concentration and illite dosage

The effects of the initial CR concentration and illite dosage on the AE were investigated. Experiments were performed at 298 K and 150 rpm using aqueous solutions with initial CR concentrations of 25 – 500 mg/L, and gradual increases in illite dosage (1 – 5 g/L). Since the highest efficiency was obtained at pH 5.7 , the initial pH of the aqueous CR solutions was adjusted accordingly. Fig. S3 shows the isotherm curves for CR adsorption onto illite. The plot indicates a Type I adsorption behavior or specifically the formation of single CR monolayers on the illite surface.

Fig. S4 shows the adsorption efficiencies and capacities obtained in the ranges of CR concentration and illite dosage tested at pH 5.7 . Yields were adversely affected by the initial CR concentration and increased with higher illite doses (Table S4). Hence, the maximum separation efficiency, 90.4% ,

Table 2
Thermodynamic parameters for the adsorption of Congo red by illite

Temperature (K)	K_L (L/mg)	ΔH° (kJ/mol)	ΔS° (J/mol·K)	ΔG° (kJ/mol)
298	0.06073			6.940
318	0.06598	-2.025	-29.7	7.186
338	0.05481			8.159

occurred at 25 mg/L CR and 5 g/L illite dosage level. On the other hand, adsorption capacity (q_e) increased at higher CR concentrations but decreased at elevated illite dosages. The maximum adsorption capacity was 61.02 mg/g, and occurred at 500 mg/L CR and an illite dosage of 1 g/L. Table 3 shows that the maximum capacity obtained with illite in this study is within the range of maximum values previously reported using different types of adsorbents for the removal of CR from aqueous solutions [12,40,62–73]. Illite has an interlayer structure and its adsorption capacity is less than montmorillonite and vermiculite, but more than kaolinite. Therefore, the cation exchange capacity (CEC) of illite is less than that of smectite (80 – 120 meq/100 g), but higher than that of kaolinite, typically around 20 – 30 meq/100 g [74].

3.7. Adsorption isotherms

Adsorption isotherms were used to examine the distribution (homogenous or heterogeneous) of CR molecules and their interactions with illite surfaces [75]. The graphs for each isotherm in Fig. 6 were obtained using the equilibrium data and the expressions of four different isotherm models [Eqs. (7)–(10)], namely, Langmuir, Freundlich, Temkin, and Dubinin–Radushkevich [76–79]. Tables 7 and S5 display the results of isotherm analysis.

$$\text{Langmuir: } \frac{C_e}{q_e} = \frac{1}{q_m \cdot K_L} + \frac{C_e}{q_m} \quad (7)$$

$$\text{Freundlich: } \log q_e = \log K_f + \left(\frac{1}{n}\right) \cdot \log C_e \quad (8)$$

Table 3
Maximum adsorption capacity (q_{\max}) values for the removal of Congo red using various adsorbents

Adsorbent	q_{\max} (mg/g)	References
Illite	61	Present study
Olive pomace	145	[12]
Amine-functionalized SBA-15	186	[40]
Montmorillonite	30	[62]
Kaolin	6	[63]
Zeolite	4	[63]
Bentonite	20	[63]
Vermiculite	298	[64]
Montmorillonite	154	[64]
Sepiolite	211	[65]
Ball-milled sugarcane bagasse	38	[66]
Guar gum/activated carbon nanocomposite	832	[67]
Waste banana peel	18	[68]
Waste orange peel	14	[68]
Bengal gram seed husk	42	[69]
Cashew nutshell	5	[70]
Raw pinecone	19	[71]
Neem leaf powder	41	[72]
Bagasse fly ash	12	[73]

$$\text{Temkin: } q_e = B_1 \cdot \ln(K_T) + B_1 \cdot \ln C_e \quad (9)$$

$$\text{Dubinin-Radushkevich: } \varepsilon = RT \ln \left(1 + \frac{1}{C_e} \right) \quad (10)$$

Fig. 6 and Table 4 show that the highest R^2 obtained with the Langmuir isotherm model (0.9994) is considerably higher than those from the Freundlich and Temkin models (0.8275 and 0.8933, respectively). This means that the adsorption of CR onto illite clay follows this model and is consistent with Fig. S3. The Langmuir maximum adsorption capacity of illite for CR adsorption was found to be 63.69 mg/g (Table 4) which is nearly identical to the experimentally-determined capacity (61.02 mg/g). The separation factor (Eq. 11), a dimensionless number of the Langmuir model (Table S5), indicates that CR adsorption onto illite is favored since R_L values range from 0.031 to 0.384 [50,80]. The trends and results observed with isotherm analysis are consistent with previous reports in the literature [81–83]. Accordingly, it is presumed that a CR monolayer is formed on the illite surface during the adsorption process. The average adsorption

energy (E) was calculated to be <8 kJ/mol, indicating that the physical or physicochemical attractions during the process follow the Dubinin–Radushkevich model [84]. These are also consistent with those obtained using thermodynamic parameters.

$$R_L = \frac{1}{(1 + K_L \cdot C_0)} \quad (11)$$

Table 4
Constants and R^2 values of the isotherm models for the adsorption of Congo red by illite

Langmuir			Freundlich		
q_{\max} (mg/g)	K_L (L/mg)	R^2	n	K_f (L/mg)	R^2
63.69	0.0607	0.9994	3.434	2.97	0.8275
Temkin			Dubinin–Radushkevich		
B_1	A_T (L/mg)	R^2	q_m (mg/g)	E (kJ/mol)	R^2
10.93	0.99	0.8933	54.00	0.158	0.8972

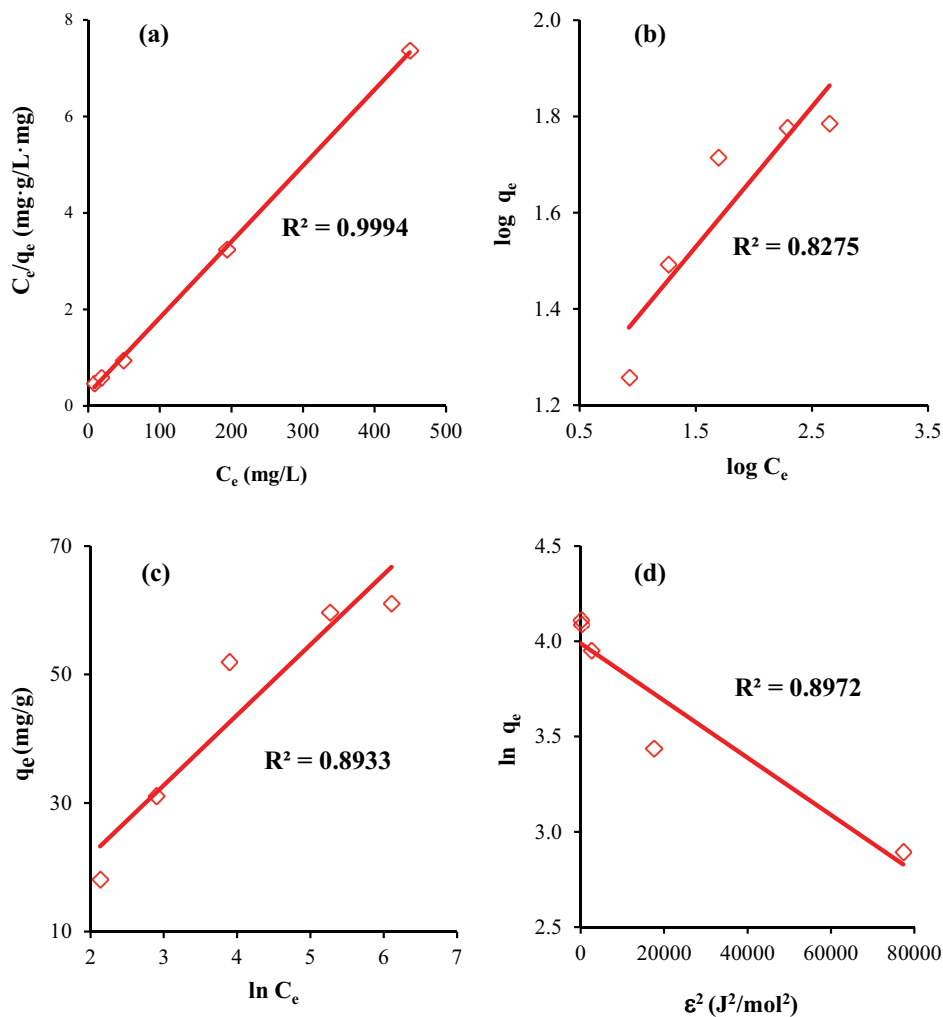


Fig. 6. Plots of isotherm models for adsorption of Congo red by illite (a) Langmuir, (b) Freundlich, (c) Temkin, and (d) Dubinin–Radushkevich.

4. Conclusion

In this study, illite was tested as an adsorbent for the removal of CR, an anionic diazo dye, from aqueous solutions. The BET surface area of the illite used was 44.73 m²/g. The results showed that the adsorption process was significantly affected by the pH of the solution and the maximum adsorption occurred at pH 5.7, while unadjusted pH of the solution was ~7.5. The reduced pH increased the electrostatic attraction of the illite and CR surface charges, thus increasing the adsorption capacity. As previously reported, the adsorption process proceeds rapidly, reaching equilibrium after 2 h. The kinetics of the process closely follow the pseudo-second-order kinetic model with an R^2 of 0.999. Elevated temperatures adversely affected the adsorption capacity, while the highest efficiency occurred at 298 K. Thermodynamic parameters showed the possible physical interactions between illite and CR. The negative ΔH° indicated the exothermic nature of the process. The isotherm curves show that the process conforms with Type 1 adsorption. Adsorption efficiency was negatively influenced by the initial CR concentration and positively affected by the adsorbent dosage. The maximum adsorption capacity ($q_e = 61.02$ mg/g) occurred at 500 mg/L CR and 1 g/L illite dosage. The equilibrium data agreed with the Langmuir isotherm model ($R^2 = 0.9994$). This study shows that illite can be used as an adsorbent to remove CR from aqueous solutions. The adsorption capacity of this mineral can be improved using several modification techniques that employ mineral acids, bases, and surfactants to improve the surface properties of the adsorbents.

Competing interest declaration

All authors declare that they have no conflict of interest.

Acknowledgements

The authors wish to acknowledge Selçuk University and Konya Technical University for the funding through the Scientific Research Projects Coordination Unit under Grant Number, 17201137.

Nomenclature and abbreviations

AE	—	Adsorption efficiency, %
B_1	—	Temkin isotherm constant, J/mol
C_o	—	Initial concentration of CR, mg/L
C_e	—	Equilibrium concentration of CR, mg/L
C_s	—	Concentration of the sample at time t , mg/L
CR	—	Congo red
E	—	Dubinin–Radushkevich energy, J/mol
I	—	Boundary layer diffusion effects (external film resistance), mg/g
k_1	—	Pseudo-first-order rate constant, 1/min
k_2	—	Pseudo-second-order rate constant, g/mg·min
k_{id}	—	Intraparticle diffusion rate constant, mg/g·min ^{0.5}
K_F	—	Freundlich adsorption capacity, L/mg
K_L	—	Langmuir equilibrium constant, L/mg

K_T	—	Temkin constant, L/mg
m	—	Mass of the illite, g
n	—	Freundlich heterogeneity constant, adsorption intensity
q_e	—	Adsorption capacity at equilibrium, mg/g
$q_{e(cal)}$	—	Calculated adsorption capacity at equilibrium, mg/g
$q_{e(exp)}$	—	Experimental adsorption capacity at equilibrium, mg/g
q_t	—	Adsorption capacity at time t , mg/g
q_{max}	—	Maximum adsorption capacity, mg/g
R	—	Gas constant, 8.314 J/mol·K
R_L	—	Langmuir dimensionless separation factor
R^2	—	Determination coefficient
t	—	Time, min
T	—	Temperature, K or °C
V	—	Volume of the aqueous CR solution, L
α	—	Elovich initial adsorption rate, mg/g·min
β	—	Elovich desorption constant, g/mg
ϵ	—	Molar extinction coefficient
[·]	—	Concentration of the species specified, mg/L
ΔG°	—	Change in Gibbs free energy, kJ/mol
ΔH°	—	Change in enthalpy, kJ/mol
ΔS°	—	Change in entropy, kJ/mol·K

References

- [1] S.C. Bhatia, Pollution Control in Textile Industry, Woodhead Publishing India Pvt. Ltd., India, 2017.
- [2] K. Ellass, A. Laachach, A. Alaoui, M. Azzi, Removal of methyl violet from aqueous solution using a stevensite-rich clay from Morocco, *Appl. Clay Sci.*, 54 (2011) 90–96.
- [3] W.C. Wanyonyi, J.M. Onyari, P.M. Shiundu, Adsorption of Congo red dye from aqueous solutions using roots of *Eichhornia crassipes*: kinetic and equilibrium studies, *Energy Procedia*, 50 (2014) 862–869.
- [4] W.G. Levine, Metabolism of azo dyes: implication for detoxication and activation, *Drug Metab. Rev.*, 23 (1991) 253–309.
- [5] A. Mittal, J. Mittal, A. Malviya, V.K. Gupta, Adsorptive removal of hazardous anionic dye “Congo red” from wastewater using waste materials and recovery by desorption, *J. Colloid Sci.*, 340 (2009) 16–26.
- [6] S.I. Siddiqui, E.S. Allehyani, S.A. Al-Harbi, Z. Hasan, M.A. Abomuti, H.K. Rajor, S. Oh, Investigation of Congo red toxicity towards different living organisms: a review, *Processes*, 11 (2023) 807, doi: 10.3390/pr11030807.
- [7] A. Mittal, L. Kurup, Column operations for the removal and recovery of a hazardous dye ‘acid red - 27’ from aqueous solutions, using waste materials—bottom ash and de-oiled soya, *Ecol. Environ. Conserv.*, 12 (2006) 181–186.
- [8] M.T. Yagub, T.K. Sen, S. Afroze, H.M. Ang, Dye and its removal from aqueous solution by adsorption: a review, *Adv. Colloid Interface Sci.*, 209 (2014) 172–184.
- [9] L.R. Bonetto, F. Ferrarini, C. de Marco, J.S. Crespo, R. Guégan, M. Giovanela, Removal of methyl violet 2B dye from aqueous solution using a magnetic composite as an adsorbent, *J. Water Process Eng.*, 6 (2015) 11–20.
- [10] H. Uslu, M.E. Marti, Equilibrium data on the reactive extraction of picric acid from dilute aqueous solutions using amberlite LA-2 in ketones, *J. Chem. Eng. Data*, 62 (2017) 2132–2135.
- [11] S. Chatterjee, M.W. Lee, S.H. Woo, Adsorption of Congo red by chitosan hydrogel beads impregnated with carbon nanotubes, *Bioresour. Technol.*, 101 (2010) 1800–1806.
- [12] K. Ali, H. Zeidan, M.E. Marti, Evaluation of olive pomace for the separation of anionic dyes from aqueous solutions: kinetic,

- thermodynamic, and isotherm studies, *Desal. Water Treat.*, 227 (2021) 412–424.
- [13] P. Saharan, V. Kumar, J. Mittal, V. Sharma, A.K. Sharma, Efficient ultrasonic assisted adsorption of organic pollutants employing bimetallic-carbon nanocomposites, *Sep. Sci. Technol.*, 56 (2021) 2895–2908.
- [14] J. Mittal, A. Mariyam, F. Sakina, R.T. Baker, A.K. Sharma, A. Mittal, Batch and bulk adsorptive removal of anionic dye using metal/halide-free ordered mesoporous carbon as adsorbent, *J. Cleaner Prod.*, 321 (2021) 129060, doi: 10.1016/j.jclepro.2021.129060.
- [15] A. Mittal, J. Mittal, A. Malviya, D. Kaur, V.K. Gupta, Adsorption of hazardous dye crystal violet from wastewater by waste materials, *J. Colloid Sci.*, 343 (2010) 463–473.
- [16] A. Mariyam, J. Mittal, F. Sakina, R.T. Baker, A.K. Sharma, A. Mittal, Efficient batch and fixed-bed sequestration of a basic dye using a novel variant of ordered mesoporous carbon as adsorbent, *Arabian J. Chem.*, 14 (2021) 103186, doi: 10.1016/j.arabj.2021.103186.
- [17] P.K. Malik, Dye removal from wastewater using activated carbon developed from sawdust adsorption equilibrium and kinetics, *J. Hazard. Mater.*, 113 (2004) 81–88.
- [18] A.A. Peláez-Cid, A.M. Herrera-González, M. Salazar-Villanueva, A. Bautista-Hernández, Elimination of textile dyes using activated carbons prepared from vegetable residues and their characterization, *J. Environ. Manage.*, 181 (2016) 269–278.
- [19] N. Boudechiche, M. Fares, S. Ouyahia, H. Yazid, M. Trari, Z. Sadaoui, Comparative study on removal of two basic dyes in aqueous medium by adsorption using activated carbon from *Ziziphus lotus* stones, *Microchem. J.*, 146 (2019) 1010–1018.
- [20] P.M. Thabede, N.D. Shoofo, E.B. Naidoo, Removal of methylene blue dye and lead ions from aqueous solution using activated carbon from black cumin seeds, *J. Chem. Eng.*, 33 (2020) 39–50.
- [21] S. Husien, R.M. El-taweel, A.I. Salim, I.S. Fahim, L.A. Said, A.G. Radwan, Review of activated carbon adsorbent material for textile dyes removal: preparation, and modelling, *Curr. Green Chem.*, 5 (2022) 100325, doi: 10.1016/j.crgsc.2022.100325.
- [22] A.A. Jalil, S. Triwahyono, M.R. Yaakob, Z.Z.A. Azmi, N. Sapawe, N.H.N. Kamarudin, H.D. Setiabudi, N.F. Jaafar, S.M. Sidik, S.H. Adam, B.H. Hameed, Utilization of bivalve shell-treated *Zea mays* L. (maize) husk leaf as a low-cost biosorbent for enhanced adsorption of malachite green, *Bioresour. Technol.*, 120 (2012) 218–224.
- [23] M.E. Marti, H. Zeidan, Evaluation of beet sugar processing carbonation sludge for the remediation of synthetic dyes from aqueous media, *Int. J. Environ. Sci. Technol.*, 20 (2023) 3875–3890.
- [24] G. Sheng, H. Dong, Y. Li, Characterization of diatomite and its application for the retention of radiocobalt: role of environmental parameters, *J. Environ. Radioact.*, 113 (2012) 108–115.
- [25] H. Tao, X. Qian, Y. Zhou, H. Cheng, Research progress of clay minerals in carbon dioxide capture, *Renewable Sustainable Energy Rev.*, 164 (2022) 112536, doi: 10.1016/j.rser.2022.112536.
- [26] S. De Gisi, G. Lofrano, M. Grassi, M. Notarnicola, Characteristics and adsorption capacities of low-cost sorbents for wastewater treatment: a review, *Sustainable Mater. Technol.*, 9 (2016) 10–40.
- [27] A.A. Adeyemo, I.O. Adeoye, O.S. Bello, Adsorption of dyes using different types of clay: a review, *Appl. Water Sci.*, 7 (2017) 543–568.
- [28] A.M. Awad, S.M. Shaikh, R. Jalab, M.H. Gulied, M.S. Nasser, A. Benamor, S. Adham, Adsorption of organic pollutants by natural and modified clays: a comprehensive review, *Sep. Purif. Technol.*, 228 (2019) 115719, doi: 10.1016/j.seppur.2019.115719.
- [29] J.L. Miao, J.Q. Ren, H.J. Li, D.G. Wu, Y.C. Wu, Mesoporous crosslinked chitosan-activated clinoptilolite biocomposite for the removal of anionic and cationic dyes, *Colloids Surf., B*, 216 (2022) 112579, doi: 10.1016/j.colsurfb.2022.112579.
- [30] N. Karakaya, M.Ç. Karakaya, A. Temel, Mineralogical and chemical properties and the origin of two types of analcime in SW Ankara, Turkey, *Clays Clay Miner.*, 61 (2013) 231–257.
- [31] X. Wang, A. Fan, A.T. (Tom) van Loon, R. Yang, Z. Han, J. Li, Chapter 11 – The Influence of Diagenesis on Low-Porosity, Low-Permeability Gas Reservoirs in the Sulige Gas Field (Ordos Basin, China), R. Yang, A.J. (Tom) Van Loon, Eds., *The Ordos Basin: Sedimentological Research for Hydrocarbons Exploration*, Elsevier, Amsterdam, 2022, pp. 191–215.
- [32] A. Meunier, B. Velde, *The Geology of Illite, Origins, Evolution and Metamorphism*, Springer, Berlin, Heidelberg, 2004.
- [33] M. Celik Karakaya, *Kil Minerallerinin Özellikleri ve Tanıtma Yöntemleri*, Selçuk University, Konya, Turkey, 2006.
- [34] M. Celik Karakaya, N. Karakaya, *Sistemik Mineraloji*, Selçuk University, Konya, Turkey, 2011.
- [35] H.H. Murray, *Applied Clay Mineralogy: Occurrences, Processing and Applications of Kaolins, Bentonites, Palygorskite-Sepiolite, and Common Clays*, H.H. Murray, Ed., *Developments in Clay Science*, Vol. 2, Elsevier, Amsterdam, 2007, 180 p.
- [36] S. Mukherjee, *Chemical Properties of Clay and Thermodynamic Aspects*, In: *The Science of Clays: Applications in Industry, Engineering and Environment*, Springer Netherlands, Dordrecht, Netherlands, 2013, pp. 46–53.
- [37] M. Celik, N. Karakaya, A. Temel, Clay minerals in hydrothermally altered volcanic rocks, Eastern Pontides, Turkey, *Clays Clay Miner.*, 47 (1999) 708–717.
- [38] L.S. Balistrieri, J.W. Murray, The surface chemistry of goethite (–FeOOH) in major ion seawater, *Am. J. Sci.*, 281 (1981) 788–806.
- [39] M.A.M. Khraisheh, M.A. Al-Ghouti, S.J. Allen, M.N. Ahmad, Effect of OH and silanol groups in the removal of dyes from aqueous solution using diatomite, *Water Res.*, 39 (2005) 922–932.
- [40] H. Zeidan, M. Can, M.E. Marti, Synthesis, characterization, and use of an amine-functionalized mesoporous silica SBA-15 for the removal of Congo red from aqueous media, *Res. Chem. Intermed.*, 49 (2023) 221–240.
- [41] G. Sedmale, M. Randers, M. Rundans, V. Seglins, Application of differently treated illite and illite clay samples for the development of ceramics, *Appl. Clay Sci.*, 146 (2017) 397–403.
- [42] J.W. Madejová, G.S. Petit, *IR Spectra of Clay Minerals, Developments in Clay Science, Infrared and Raman Spectroscopies of Clay Minerals*, Elsevier, Amsterdam, 2017, pp. 107–149.
- [43] F.M. Machado, C.P. Bergmann, T.H.M. Fernandes, E.C. Lima, B. Royer, T. Calvete, S.B. Fagan, Adsorption of Reactive Red M-2BE dye from water solutions by multi-walled carbon nanotubes and activated carbon, *J. Hazard. Mater.*, 192 (2011) 1122–1131.
- [44] N. Karakaya, M.Ç. Karakaya, K. Faure, Doğu Karadeniz Bölgesi kil mineralleşmelerinin oluşumu ve kökeni, *Selçuk Univ. Müh. Bilim Teknol. Derg.*, 22 (2007) 1–12.
- [45] V. Ponnusami, S. Vikram, S.N. Srivastava, Guava (*Psidium guajava*) leaf powder: novel adsorbent for removal of methylene blue from aqueous solutions, *J. Hazard. Mater.*, 152 (2008) 276–286.
- [46] S. Dadou, T. Berrama, N. Doufene, C. Zekkaoui, A. Beriber, Evaluating untreated clay's adsorptive capacity to remove an anionic dye from aqueous solution, *Arabian J. Sci. Eng.*, 44 (2019) 9889–9903.
- [47] C.H. Weng, Y.F. Pan, Adsorption of a cationic dye (methylene blue) onto spent activated clay, *J. Hazard. Mater.*, 144 (2007) 355–362.
- [48] Y. Omid Khaniabadi, H. Basiri, H. Nourmoradi, M.J. Mohammadi, A.R. Yari, S. Sadeghi, A. Amrane, Adsorption of Congo red dye from aqueous solutions by montmorillonite as a low-cost adsorbent, *Int. J. Chem. React. Eng.*, 16 (2017) 20160203, doi: 10.1515/ijcre-2016-0203.
- [49] K.L. Tan, B.H. Hameed, Insight into the adsorption kinetics models for the removal of contaminants from aqueous solutions, *J. Taiwan Inst. Chem. Eng.*, 74 (2017) 25–48.
- [50] H. Zeidan, M.E. Marti, Separation of formic acid from aqueous solutions onto anion exchange resins: equilibrium, kinetic, and thermodynamic data, *J. Chem. Eng. Data*, 64 (2019) 2718–2727.
- [51] S. Lagergren, Zur theorie der sogenannten adsorption gelöster stoffe, *Kungliga svenska vetenskapsakademiens, Handlingar*, 24 (1898) 1–39.

- [52] Y.S. Ho, G. McKay, Pseudo-second-order model for sorption processes, *Process Biochem.*, 34 (1999) 451–465.
- [53] S.Y. Elovich, O. Larinov, Theory of adsorption from solutions of non-electrolytes on solid (I) equation adsorption from solutions and the analysis of its simplest form, (II) verification of the equation of adsorption isotherm from solutions, *Izv. Akad. Nauk. SSSR, Otd. Khim. Nauk.*, 2 (1962) 209–216.
- [54] W.J. Weber, J.C. Morris, *Water Pollution Symposium, Proceedings of 1st International Conference on Water Pollution Research*, Pergamon Press, Oxford, 1962, pp. 231–266.
- [55] G.M. Walker, L. Hansen, J.A. Hanna, S.J. Allen, Kinetics of a reactive dye adsorption onto dolomitic sorbents, *Water Res.*, 37 (2003) 2081–2089.
- [56] V. Vimonses, S. Lei, B. Jin, C.W.K. Chow, C. Saint, Kinetic study and equilibrium isotherm analysis of Congo red adsorption by clay materials, *J. Chem. Eng.*, 148 (2009) 354–364.
- [57] O.S. Omer, M.A. Hussein, B.H.M. Hussein, A. Mgaidi, Adsorption thermodynamics of cationic dyes (methylene blue and crystal violet) to a natural clay mineral from aqueous solution between 293.15 and 323.15 K, *Arabian J. Chem.*, 11 (2018) 615–623.
- [58] H. Zeidan, D. Ozdemir, N. Kose, E. Pehlivan, G. Ahmetli, M.E. Marti, Separation of formic acid and acetic acid from aqueous solutions using sugar beet processing fly ash: characterization, kinetics, isotherms, and thermodynamics, *Desal. Water Treat.*, 202 (2020) 283–294.
- [59] D.M. Ruthven, *Principles of Adsorption and Adsorption Processes*, John Wiley & Sons, New York (USA), 1984.
- [60] L. Cottet, C.A.P. Almeida, N. Naidek, M.F. Viante, M. Lopes, N. Debacher, Adsorption characteristics of montmorillonite clay modified with iron oxide with respect to methylene blue in aqueous media, *Appl. Clay Sci.*, 95 (2014) 25–31.
- [61] K. Chinoune, K. Bentaleb, Z. Bouberka, A. Nadim, U. Maschke, Adsorption of reactive dyes from aqueous solution by dirty bentonite, *Appl. Clay Sci.*, 123 (2016) 64–75.
- [62] L. Wang, A. Wang, Adsorption characteristics of Congo red onto the chitosan/montmorillonite nanocomposite, *J. Hazard. Mater.*, 147 (2007) 979–985.
- [63] V. Vimonses, S. Lei, B. Jin, C.W.K. Chow, C. Saint, Kinetic study and equilibrium isotherm analysis of Congo red adsorption by clay materials, *Chem. Eng. J.*, 148 (2009) 354–364.
- [64] F. Ding, M. Gao, T. Shen, H. Zeng, Y. Xiang, Comparative study of organo-vermiculite, organo-montmorillonite and organo-silica nanosheets functionalized by an ether-spacer-containing Gemini surfactant: Congo red adsorption and wettability, *Chem. Eng. J.*, 349 (2019) 388–396.
- [65] J. Zhang, Z. Yan, J. Ouyang, H. Yang, D. Chen, Highly dispersed sepiolite-based organic modified nanofibers for enhanced adsorption of Congo red, *Appl. Clay Sci.*, 157 (2018) 76–85.
- [66] L. Zhang, L. Moghaddam, I.M. O'Hara, W.O.S. Doherty, Congo red adsorption by ball-milled sugarcane bagasse, *Chem. Eng. J.*, 178 (2011) 122–128.
- [67] V.K. Gupta, S. Agarwal, R. Ahmad, A. Mirza, J. Mittal, Sequestration of toxic Congo red dye from aqueous solution using ecofriendly guar gum/activated carbon nanocomposite, *Int. J. Biol. Macromol.*, 158 (2020) 1310–1318.
- [68] G. Annadurai, R.L. Juang, D.J. Lee, Use of cellulose-based wastes for adsorption of dyes from aqueous solutions, *J. Hazard. Mater.*, 92 (2002) 263–274.
- [69] M.C.S. Reddy, V. Nirmala, C. Ashwini, Bengal gram seed husk as an adsorbent for the removal of dye from aqueous solutions—batch studies, *Arabian J. Chem.*, 10 (2017) 2554–2566.
- [70] P.S. Kumar, S. Ramalingam, C. Senthamarai, M. Niranjana, P. Vijayalakshmi, S. Sivanesan, Adsorption of dye from aqueous solution by cashew nut shell: studies on equilibrium isotherm, kinetics and thermodynamics of interactions, *Desalination*, 261 (2010) 52–60.
- [71] S. Dawood, T.K. Sen, Removal of anionic dye Congo red from aqueous solution by raw pine and acid-treated pine cone powder as adsorbent: equilibrium, thermodynamic, kinetics, mechanism and process design, *Water Res.*, 46 (2012) 1933–1946.
- [72] K.G. Bhattacharyya, A. Sharma, *Azadirachta indica* leaf powder as an effective biosorbent for dyes: a case study with aqueous Congo red solutions, *J. Environ. Manage.*, 71 (2004) 217–229.
- [73] I.D. Mall, V.C. Srivastava, N.K. Agarwal, I.M. Mishra, Removal of Congo red from aqueous solution by bagasse fly ash and activated carbon: kinetic study and equilibrium isotherm analyses, *Chemosphere*, 61 (2005) 492–501.
- [74] N. Kumari, C. Mohan, *Basics of Clay Minerals and Their Characteristic Properties*, G.M.D. Nascimento, Ed., *Clay and Clay Minerals*, InTechOpen, 2021, pp. 1–29.
- [75] C.A.P. Almeida, N.A. Debacher, A.J. Downs, L. Cottet, C.A.D. Mello, Removal of methylene blue from colored effluents by adsorption on montmorillonite clay, *J. Colloid Interface Sci.*, 332 (2009) 46–53.
- [76] I. Langmuir, The constitution and fundamental properties of solids and liquids, Part I. Solids, *J. Am. Chem. Soc.*, 38 (1916) 2221–2295.
- [77] H. Freundlich, Über die adsorption in lösungen, *Zeitschrift für physikalische Chemie.*, 57 (1907) 385–470.
- [78] M. Temkin, Kinetics of ammonia synthesis on promoted iron catalysts, *Acta Physiochim.*, URSS, 12 (1940) 327–356.
- [79] M.M. Dubinin, L.V. Radushkevich, Evaluation of microporous materials with a new isotherm, In *Dokl. Akad. Nauk. SSSR*, 55 (1947) 331–334.
- [80] M. Momina, M. Shahadat, S. Ismail, Regeneration potential of bentonite-based Paintosorp™ for removal of industrial dye, *Arabian J. Sci. Eng.*, 45 (2020) 551–561.
- [81] A.M. Ashrul, M.S.M. Sahid, K.M. Padmosoedarso, A.H. Mahadi, E. Kusri, J. Hopley, A. Usman, Individual and competitive adsorption of negatively charged Acid Blue 25 and Acid Red 1 onto raw Indonesian kaolin clay, *Arabian J. Sci. Eng.*, 47 (2022) 6617–6630.
- [82] P.H. Chang, J. Guo, J. Li, Z. Li, X. Li, Seizing forbidden drug ranitidine by illite and the adsorption mechanism study, *Colloids Surf., A*, 639 (2022) 128395, doi: 10.1016/j.colsurfa.2022.128395.
- [83] B.A.M. Fil, M. Korkmaz, C. Özmetin, Application of nonlinear regression analysis for methyl violet (MV) dye adsorption from solutions onto illite clay, *J. Dispersion Sci. Technol.*, 37 (2016) 991–1001.
- [84] C. Saka, Ö. Sahin, Removal of methylene blue from aqueous solutions by using cold plasma-and formaldehyde-treated onion skins, *Color. Technol.*, 127 (2011) 246–255.

Supporting information

Table S1
Properties of Congo red

Dye name	Congo red
CAS No.	573-58-0
Empirical formula	$C_{32}H_{22}N_6Na_2O_6S_2$
Molecular weight	696.7 g/mol
Melting point	36°C
Water solubility	3.3 g/100 mL (25°C)
Functional group	SO_3^-
Ionization constant (pKa)	4.5

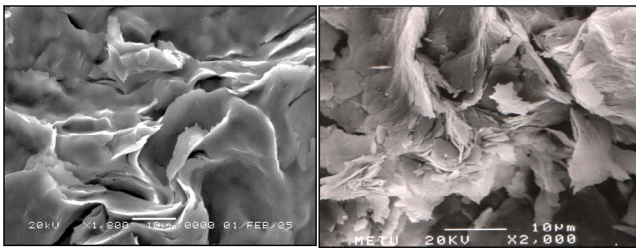


Fig. S1. SEM images of illite samples.

Table S2
Chemical composition of the illite used in this study

Compound	Percent (wt.%)
SiO ₂	51.43
Al ₂ O ₃	31.41
Fe ₂ O ₃	0.68
MgO	0.59
CaO	0.98
Na ₂ O	0.20
K ₂ O	7.98
TiO ₂	0.19
LOI	6.51
Total	99.97

Table S3
Semi-quantitative elemental composition of the illite used in this study

Element	wt. (%)
O	46.34
Si	22.39
Al	19.42
K	8.21
Mg	1.08
C	0.89
Fe	0.77
Ti	0.32
S	0.24
Na	0.33

Table S4
Significance of various parameters on the adsorption of Congo red onto illite

Parameter	p-value	f-value
pH	0.0035	37.9
Contact time	4.8×10^{-8}	383.3
Initial concentration	1.7×10^{-6}	40.5
Illite dose	0.0109	7.7
Temperature	0.9811	6×10^{-4}

p-value < 0.05, f-value > 5: significant.
p-value > 0.05, f-value < 5: insignificant.

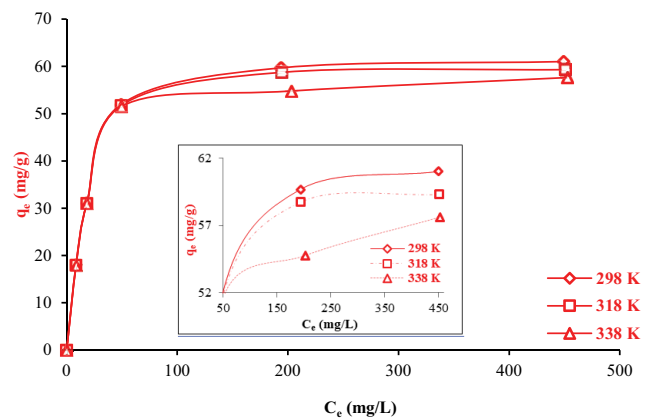


Fig. S2. Effect of temperature on adsorption of Congo red by illite ([CR] = 100 mg/L, dose = 1 g/L, pH = 5.7).

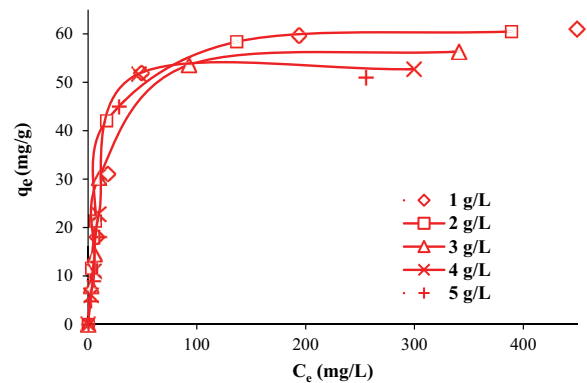


Fig. S3. Isotherm curves for adsorption of Congo red by illite (pH = 5.7, T = 298 K).

Table S5
Separation factor (R_L) values calculated for the adsorption of Congo red by illite

Dye concentration (mg/L)	R_L
25	0.384
50	0.250
100	0.140
250	0.061
500	0.031

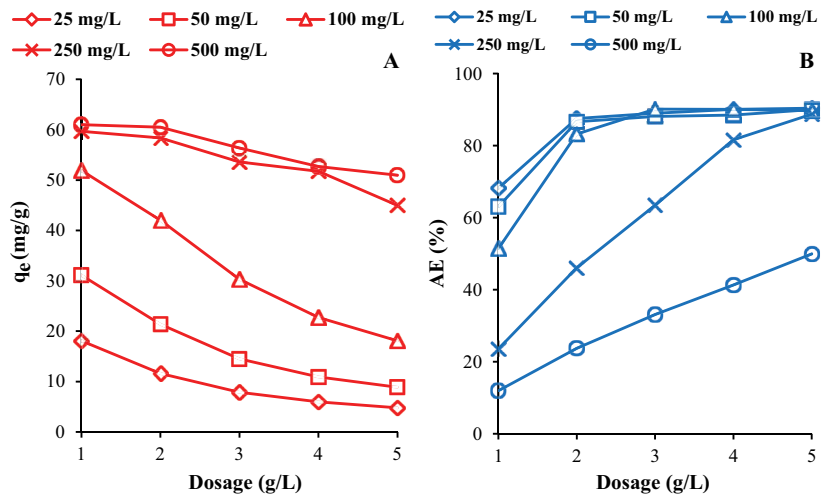


Fig. S4. Effects of Congo red concentration and illite dosage on adsorption of Congo red by illite q_e vs. dosage, (b) adsorption efficiency vs. dosage ($T = 298$ K, $pH = 5.7$).